Journal of Thermal Analysis and Calorimetry
https://doi.org/10.1007/s10973-021-10939-4

Hydration of high-alumina calcium aluminate cements with carbonate and sulfate additives

Jonathan Lapeyre[1] · Sai Akshay Ponduru[1] · Monday Okoronkwo[2] · Hongyan Ma[3] · Aditya Kumar[1]

Received: 25 July 2020 / Accepted: 7 June 2021

Abstract
This study investigated the influence of limestone (LS) and calcium sulfate (C$) mineral additives on the hydration kinetics of high-α-Al_2O_3 calcium aluminate cement (CAC) utilizing experimental techniques and thermodynamic simulations. Increasing the replacement level of limestone or calcium sulfate increased the cumulative heat of the hydration reaction. The limestone exhibited limited acceleratory effects to the CAC hydration kinetics due to the coarseness of the powder. The coarse particle size distribution limited any heterogenous nucleation that would have occurred with a finer particle size as well as the intrinsic insolubility kinetically limits the formation of monocarboaluminate phases. Conversely, the cumulative heat release increased as the limestone content increased; however, this was not due to any enhanced reactivity provided by the limestone. Instead, this increase in the cumulative heat is due to a combination of the LS and the increase in the amount of water available to react with CAC via the dilution effect. In comparison, the increase in the C$ replacement level accelerated the heat flow rate of CAC with the C$ particles acting as a favorable surface for heterogenous nucleation of the hydrates during the initial stages of the hydration reaction. Increasing the C$ replacement level does not form more ettringite and does not translate in an increase in the compressive strength. After the 72-h hydration period, C$ remains in the microstructure, showing that the complete dissolution of C$ is not responsible for the monotonic increase in heat flow rate. It is expected that the amount of hydrates or residual unreacted particles cannot compensate for the decrease in strength caused by the reduction of α-Al_2O_3 present in the CAC.

Keywords Calcium aluminate cement · Hydration kinetics · Filler effect · Thermodynamics

Introduction

Calcium aluminate cement (CAC) is a hydraulic binder that provides many advantages like enhanced abrasion resistance, resistance to biogenic corrosion, low permeability, and rapid hardening compared to hardened ordinary Portland cement (OPC). Even though CACs exhibit these superior properties, the usage of CACs outside of niche applications such as refractory castables, wastewater or sewers linings, dental applications, among others is limited due to the higher price of CAC compared to OPC [1–3].

Monocalcium aluminate ($CaAl_2O_4$, CA) is the main phase present in CACs and is the most reactive phase compared to the other prominent calcium aluminate phases such as CA_2, $C_{12}A_7$, and/or C_4AF present in CAC. For convenience, cement chemistry shorthand for the cementitious compounds and constituent oxides is utilized (e.g., $CaAl_2O_4$ = CA and CaO = C, Al_2O_3 = A, $CaSO_4$ = $, respectively). These reactants form different hydrate phases depending on the duration of the hydration reaction or the temperature conditions during the hydration reaction. The temporal evolution of these hydration products is called the "conversion" process. The conversion process is the time-dependent transformation of metastable calcium aluminate hydrate phases: calcium aluminate decahydrate ($CaAl_2O_4{\cdot}10H_2O$, CAH_{10}) and hydroxyl-AFm [C_2AH_x where x is moles of H_2O which is reported to vary from 7, or 8 mol; for this manuscript, 8 mol

✉ Aditya Kumar
kumarad@mst.edu

1 Department of Materials Science and Engineering, Missouri University of Science and Technology, Rolla, MO, USA

2 Department of Chemical and Biochemical Engineering, Missouri University of Science and Technology, Rolla, MO, USA

3 Department of Civil, Architectural and Environmental Engineering, Missouri University of Science and Technology, Rolla, MO, USA

Published online: 26 June 2021

is assumed to be present [4, 5]]; eventually, these phases transforms into the thermodynamically stable phase: hydrogarnet ($Ca_3Al_2(OH)_{12}$, C_3AH_6). Additionally, amorphous aluminum hydroxide gel ($Al(OH)_3$, AH_3) forms during the hydration of CAC phases. The result of the conversion process is the metastable CAH_{10} and C_2AH_8 phases that release free water (i.e., non-chemically bound water) as C_3AH_6 forms, increasing the density of the hydrate (the density of the stable C_3AH_6 is 2.52 g cm^{-3} compared to 1.72 g cm^{-3} and 1.95 g cm^{-3} for CAH_{10} and C_2AH_8, respectively) [6]. This transformation reduces the volume of hydrates and reduces the connectivity of the hydrates in the microstructure causing a significant increase in the porosity, decreasing the strength of the bulk material. Separate from the conversion process, there are several temperature regimes in which certain reactions are thermodynamically favored, and therefore, certain calcium aluminate hydrates are predominant. Between 0 and 20 °C CAH_{10} forms, 20–35 °C C_2AH_8 forms, and above 35 °C C_3AH_6 forms [7]. For simplicity, the hydration of CA for different reactions as well as the conversion process for those temperatures is shown in Eqs. 1–3. The other clinker phases undergo similar reaction but require longer timeframes due to the other phases being intrinsically less reactive [8, 9]. When CA reacts in lower temperature regimes (shown in Eqs. 1a and 2a), metastable CAH_{10} initially forms but given enough time, CAH_{10} decomposes into C_2AH_8, AH_3 and free water. Subsequently the C_2AH_8 hydrate can transform into C_3AH_6 as seen in Eq. 2b. Similarly, for temperate temperatures, the CA hydrates form C_2AH_8 from the onset of the hydration reaction in addition to AH_3 but later, the C_2AH_8 converts in the C_3AH_6, AH_3 and free water. Equation 3 is the higher-temperature case where C_3AH_6 forms outright instead of the metastable hydrates. The experiments herein were conducted near room temperature (i.e., 20–25 °C); therefore, the CAH_{10} and hydroxyl-AFm phases are expected to form.

$T \leq 20$ °C

$$CA + 10H \rightarrow CAH_{10} \quad (1a)$$

$$2CAH_{10} \rightarrow C_2AH_8 + AH_3 + 9H \quad (2a)$$

$20\ °C \leq T \leq 35\ °C$

$$2CA + 11H \rightarrow C_2AH_8 + AH_3 \quad (1b)$$

$$3C_2AH_8 \rightarrow 2C_3AH_6 + AH_3 + 9H \quad (2b)$$

$T \geq 35$ °C

$$3CA + 12H \rightarrow C_3AH_6 + 2AH_3 \quad (3)$$

To avoid the conversion process, many researchers have replaced CAC with additives such as limestone, silica fume, and blast furnace slag that to react with hydroxyl-AFm (aluminate-ferrite-mono) to form other AFm phases or suppress the formation of the CAH_{10} [9–13]. The general formula for AFm phases (or layered double hydroxides in other scientific fields [14, 15]) can be described as $[Ca_2Al(OH)_6]^+ \cdot A^- \cdot nH_2O$ where A is an anionic species such as OH^- and n represents the number of moles of water [16, 17]. To obtain charge balance, several anions species can coordinate with the positive calcium aluminate complex forming the AFm hydrate; some examples of the anionic species and the respective of AFm phases that form in cement are aluminosilicate $\left[AlSi(OH)_8\right]^-$ forming strätlingite, sulfate (SO_4^{2-}) forming monosulfoaluminate, hydroxyl-carbonate $\left[(OH)(CO_3)_{0.5}\right]^-$ forming hemicarboalumiante, and carbonate (CO_3^{2-}) forming monocarboaluminate, respectively [4, 5, 18, 19]. In this study, two binary mix designs will be investigated: calcium aluminate cement mixed with limestone [CAC + LS] as well as calcium aluminate cement with anhydrous calcium sulfate [CAC + C$]. The corresponding AFm phases associated with these additives are hemicarboaluminate and monocarboaluminate for the limestone mix designs, while monosulfoaluminate is expected to form with the mixtures containing calcium sulfate.

The reaction between limestone and CAC is shown in Eqs. 4 and 5. The difference between hemicarboaluminate and monocarboaluminate is dependent on the initial carbonate content of the mixture. As the initial carbonate chemical concentration increases [quantified via the ratio of $CO_3/(CO_3 + 2OH^-)$ in [4]], the prominent hydration products changes from the hydroxyl-AFm phase to hemicarboaluminate and then monocarboaluminate [4, 20].

$$3CA + 0.5CaCO_3 + 18H \rightarrow C_4A(CO_3)_{0.5}H_{12} + 2AH_3 \quad (4)$$

$$3CA + CaCO_3 + 17H \rightarrow C_4A(CO_3)H_{11} + 2AH_3 \quad (5)$$

Conversely, the reaction in the [CAC + C$] system initially forms ettringite with amorphous aluminum hydroxide as shown in Eq. 6. If the calcium sulfate is depleted and excess CA is available, the ettringite is consumed to form monosulfoaluminate; see Eq. 7. The thermodynamic stability of these AFm phases varies with temperature and/or the anionic species, but it is understood that the carbonate AFm phases are more thermodynamically stable than the monosulfoaluminate phase followed by the metastable hydroxyl-AFm [4].

$$3CA + 3C\$ + 38H \rightarrow C_6A\$_3H_{32} + 2AH_3 \quad (6)$$

$$6CA + C_6A\$_3H_{32} + 16H \rightarrow 3C_4A\$H_{12} + 4AH_3 \quad (7)$$

In addition to reducing the amount of metastable CAH_{10} or hydroxyl-AFm phases, the replacement of CAC with fine

additives can prompt beneficial effects to the hydration kinetics. In OPC systems, it is well understood that fine additives can enhance the reaction rates during the initial stages of the hydration reaction by prompting the heterogeneous nucleation of the hydrates known as the filler effect [21–25]. CAC systems experience similar benefits as observed in the works of Puerta-Falla et al. and Klaus et al. [10, 26] in which increasing the total specific surface area of the paste decreased the low heat rate period and increase the cumulative heat release of the system. In contrast to OPC systems, where limestone appears to be a more effective filler than quartz [22, 27, 28], both carbonate and quartz fillers exhibit similar benefits to the hydration kinetics of CAC [10]. Likewise, the fineness of additives such as C$ in [$C_3A+C\$$] systems can influence the rate of which the ettringite and monosulfoaluminate reactions (Eqs. 6 and 7) occur [29–31]. The objective for this study is to investigate the effects of replacing a commercial high-α-Al_2O_3 calcium aluminate cement with limestone or calcium sulfate and observe the change in the hydration kinetics due to these additives (or combination of any beneficial effects introduced with these mineral additives) as well as utilizing both characterization methods and thermodynamic simulations to gain insight into how these additives can affect the hydration kinetics, phase composition, and strength of the bulk material.

Materials and methods

Commercially available high-alumina calcium aluminate cement CA-25 C (Almatis, Rotterdam, the Netherlands) was used for this study. The cement composition was measured using a X-Supreme8000 (Oxford Instruments, Aubney Woods, Abingdon, UK) X-ray fluorescence (XRF) device using a tungsten X-ray source. The result shown in Table 1. A modified method included with the device was used to determine the composition. The standardless method was adjusted using a NIST Standard Reference Material 2690 coal fly ash. Likewise, instead of measuring the powders in air, the atmosphere was replaced with helium to prevent fluorescence measurements from gases such as argon. X-ray diffraction (XRD) was utilized and confirmed that the cementitious phases present were CA, CA_2, $C_{12}A_7$, and corundum (i.e., α-Al_2O_3), a non-cementitious phase added to enhance properties at elevated temperatures. Like OPC, there are different types of CAC cements with varying cement compositions tailored for different applications. The CA-25 C would fall under the "high-alumina" category reserved for refractory applications, while other types conversely have less alumina and higher concentrations of other oxides such as CaO, SiO_2, Fe_2O_3+FeO, and TiO_2 for "finishing" or other applications [1].

Similarly, the limestone ($CaCO_3$, LS) powders and anhydrous calcium sulfate ($CaSO_4$, C$) powders are commercially available from Mississippi Lime Company (St. Louis, MO USA) and Alfa Asear (Tewksbury, MA USA), respectively. The powders were used as received, and no additional powder processing or grinding processes were utilized. The particle size distribution (PSD) of each of the solid particles were measured using a Microtrac (York, PA USA) S3500 particle size analyzer. The volumetric distribution of each powder is shown in Fig. 1. These powders were immersed in isopropyl alcohol and subsequently ultrasonically agitated to enhance dispersion of the mixture before measuring.

The median particle sizes (d_{50}, μm) of the CAC, C$, and LS were determined as 15.17 μm, 42.15 μm, and 9.99 μm, respectively. Using both the respective densities (3.29 g cm^{-3}, 2.97 g cm^{-3}, and 2.71 g cm^{-3} for CAC, C$, and LS, respectively) and PSDs of the powders, the specific surface area (SSA) for the powders was calculated as 3690 kg m^{-3}, 4091 kg m^{-3} and 2370 kg m^{-3} for CAC, C$, and LS, respectively. These calculations assume the individual particles are smooth and solid (i.e., no exterior roughness nor internal porosity) [23, 24]. The SSA is slightly underestimated by a factor of × 1.6 to × 2.2 compared to Brunauer–Emmett–Teller (BET) method [32, 33].

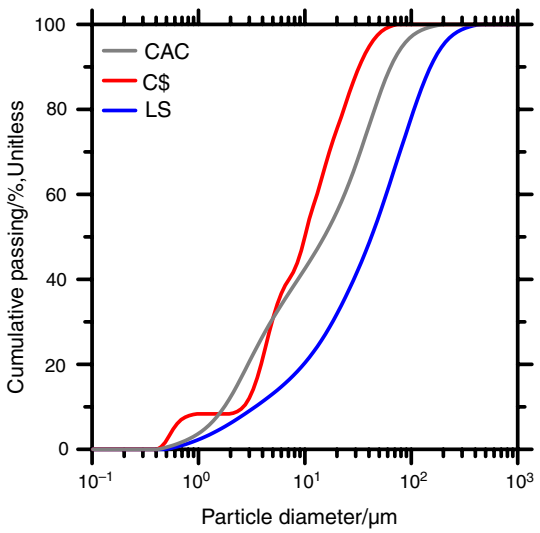

Fig. 1 Particle size distribution of the calcium aluminate cement (CAC), calcium sulfate (C$), and limestone (LS). The d_{50} for those powders are 15.17 μm, 9.99 μm, and 42.15 μm, respectively

Table 1 Chemical composition by mass percent (mass%) of CA-25-C determined via XRF

Oxide	Al_2O_3	CaO	SiO_2	MgO	Na_2O	Fe_2O_3
mass%	81.00	18.00	0.176	0.235	0.471	0.118

All the pastes were prepared by mixing the total solids with deionized water (18.3 MΩ) at a constant liquid-to-solid ratio (*l*/*s*) of 0.45. It should be noted that in the *l*/*s* ratio, the "solid" is the summation of CAC plus additive (if the latter is present in that mix design). The replacement level was as follows by mass basis 0%, 9%, 17%, 20%, 25%, 33%, and 50%. The hydration kinetics of the CAC and binary CAC pastes were monitored for a 72-h hydration period after mixing in an I-Cal 8000 (Calmetrix, USA). The calorimeter is programmed to maintain a constant temperature at 25 °C within the testing period. Finally, a series of strength measurements were taken using an Instron-5881 (Norwood, MA USA) with a 0.5 mm mm^{-1} rate. Cubic samples $6 \times 6 \times 6$ mm^3 were cast in customized silicone molds and placed in a humid chamber at room temperature for three days. For the strength results, both the average strength and standard deviation for the pure CAC paste as well as 17%, 25%, and 50% for both [CAC + LS] and [CAC + C$] are reported herein.

The characterization of the pastes was conducted through differential thermogravimetric analysis (DTGA) and X-ray diffraction (XRD) on pastes hydrated for 72 h. Isopropyl alcohol (IPA) was used to arrest the hydration process via the solvent exchange method [34, 35]. For the DTGA, a Q600 SDT (TA Instruments, New Castle, DE) instrument was used with temperature and mass sensitivity of 0.25 °C and 0.1 µg, respectively. The crushed CAC or binary CAC pastes were immersed in IPA for 24 h before drying in an electric drying oven at 60 °C for an hour. The DTGA apparatus was heated starting at 25 °C with a heating rate of 10 °C per minute in Al_2O_3 crucibles up to a maximum temperature of 1000 °C. The XRD for the binary CAC systems was prepared using sliced sections method as described [36], likewise a Panalytical X'Pert PRO in continuous scan mode with fixed divergence slit size of 0.125° was utilized. A scan step size of 0.03°2θ between the scanning range of 5.025°2θ to 89.985°2θ was utilized with a Kα_1 wavelength = 1.54056 Å. The X-ray tube was operated at a voltage of 45 kV and a current of 40 mA. The pure CAC paste was measured via Panalytical X'Pert Pro multi-purpose diffractometer using the following measurement parameters: fixed divergence slit size of 0.38°, scan step 0.0262°, and Kα_1 wavelength = 1.540598 Å with the same voltage, tube current, and scanning range. Due to these differences, quantitative comparisons of the intensities will not be made between the pure CAC pastes and the binary CAC pastes.

Coupled with these experimental methods, a series of thermodynamic calculations were made to predict the composition of the paste microstructure. This was carried out utilizing the GEM-Selektor (Gibbs Energy Minimization Software for Geochemical Modeling, version 3.4) platform in conjunction with Cemdata18 thermodynamic database [37–39]. The simulated CAC was represented in the form of simple oxides for the CAC precursor (e.g., CaO, Al_2O_3) as determined through the XRF dataset utilized in Table 1. These simulated solids in addition to water were utilized as the input to calculate the product phases as the hydration reaction occurs. For the sake of simplicity, these simulations are conducted with a 1:1 water-to-total solid ratio so that the simulations can run until the CAC has completely hydrated. This prevents inconsistencies where there is not enough water for the CAC or binary CAC pastes to completely react.

Results and discussion

Figure 2 shows the heat evolution calorimetry of the CAC as well as the binary [LS + CAC] paste. The effect of the limestone additions does not appear to accelerate the heat flow rate at either the first or second hydration peak. These results are similar to the study by Cook et al. [25] in which C_3S was partially replaced with LS that had a similar reported PSD (d_{50} reported was 43.35 µm). The benefits of coarse LS were not as high compared to the other finer filler additives

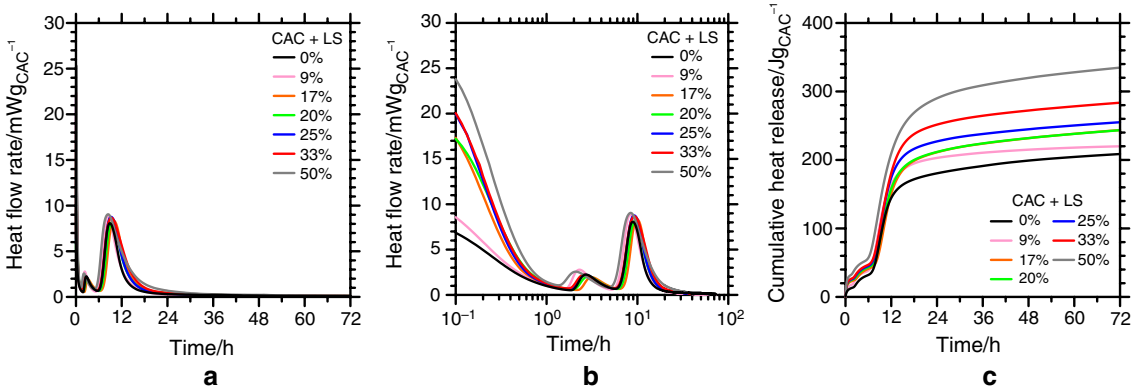

Fig. 2 Calorimetry profiles of [CAC + LS] pastes with increasing percent of CAC replaced with LS. **a** Heat flow rate up to 72 h with linear axis, **b** heat flow rate with logarithmic x-axis and **c** cumulative heat release of the [CAC + LS] pastes

within that same paper or other investigations [10, 22, 24, 25]. Examining the first hydration peak via Fig. 2b, any early acceleratory effects that could be attributed to heterogeneous nucleation before 10 h are limited. Likewise, the addition of LS does not appear to accelerate the formation of the second peak present at 10 h, but some broadening is observed. While the heat flow rates between the different LS replacement levels are similar, the cumulative heat release increases as the replacement level increases. This will be examined more in depth and compared to the [CAC + C$] calorimetry curves in the discussion of Figs. 4 and 5.

The effect of the heat flow rate with the varying C$ replacement level is shown in Fig. 3. Compared to the [CAC + LS] mixtures, the first peak exhibits a monotonic increase in the heat flow rate as well as a leftward shift as the C$ replacement level increases. This is contrary in [C_3A + C$] systems, where the [CAC + C$] pastes do not have a positive correlation between the C$ replacement level and the time to the ettringite peak [29–31, 40]. Although the exact mechanism in the [C_3A + C$] systems is hypothesized as some surface passivation mechanism [29, 41–43], the effect does not appear to correlate with the increasing C$ replacement levels in Fig. 3. There appears to be a rightward (i.e., delayed) shift in the second peak with the highest and lowest replacement level (50% and 9%, respectively), but the remaining binary pastes experience a slight leftward shift at the second peak. At later times approaching ≈ 20 h, a third heat flow rate peak appears for some of the [CAC + C$] pastes (e.g., 17%, 20%, 25%, and 33% replacement levels). A complimentary heat flow rate peak is not seen in the [CAC + LS] pastes. This calorimetry peak is likely associated with the formation of monosulfoaluminate as observed previously in the literature, and the XRD results are presented later in Fig. 7 [29–31]. The cumulative heats released for the [CAC + C$] pastes increase as the C$ content increases; however, it does not appear to simply be shifted upwards like the [CAC + LS] paste. Comparing the calorimetry curves of the binary pastes could elucidate the origins of these effects in the binary LS and C$ systems.

To quantitatively compare the CAC pastes with the LS and C$ binary systems, certain calorimetric parameters were extracted from the calorimetry profiles and were plotted with respect to the additive replacement level. These parameters were the heat flow rate of both first and second heat flow rate peaks as well as the inverse time to those corresponding peaks. As shown in Fig. 4a, b focusing on the first peak, the addition of LS does not prompt an increase nor a decrease (except at 9% replacement) for the heat flow rate or the inverse time to peak. It is expected that the coarse LS powders limit any benefit via the filler effect; this is compounded with the intrinsic low solubility limiting any chemical reactivity [9, 10, 44]. On the other hand, the increase in C$ replacement level increases the heat flow rate and accelerates (i.e., prompts a leftward shift) the first heat flow rate curve reaching the first peak within first three hours. The fineness of the C$ particles as well as dissolution of C$ could be factors in the early enhancements of the calorimetry curve. Both the high specific surface area and intrinsic solubility of C$ both favor the heterogenous nucleation and growth of ettringite which is known to occur very rapidly during the initial stages of hydration [29, 30, 45]; however, calorimetry by itself cannot elucidate the degree of which one or the other is occurring. For the second peak, there is no positive or negative correlation as the replacement level increases. Although the 9% and 50% C$ replacement level do delay the second hydration peak, it is not consistent as the replacement level increases. After the initial hydration peak, the beneficial effects provided by the C$ powder are limited. This can be attributed to the complete dissolution of the C$ or, in addition to dissolution, any removal of any reactive surface area previously available for dissolution and/

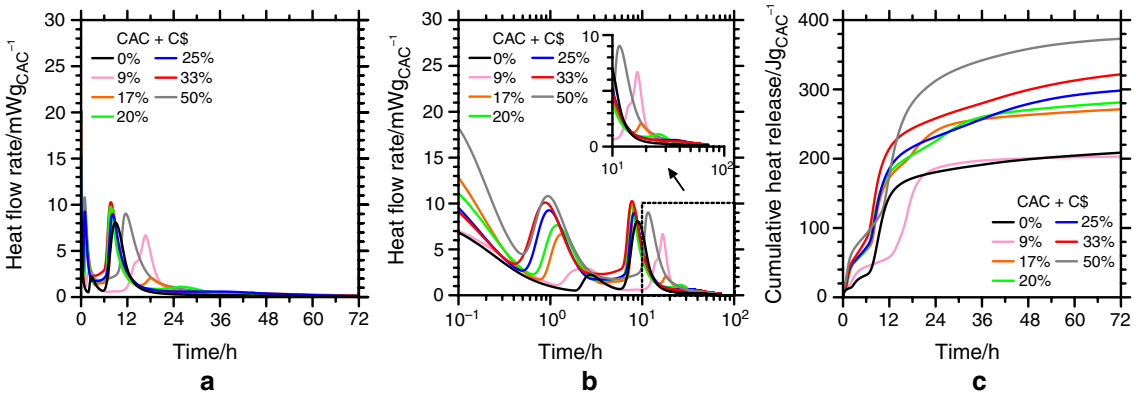

Fig. 3 Calorimetry profiles of [CAC + C$] pastes with increasing percent of CAC replaced with C$. **a** heat flow rate up to 72 h with linear axis, **b** heat flow rate with logarithmic x-axis focus on the first peak and inset for peaks after 10 h, **c** cumulative heat release of the [CAC + C$] pastes

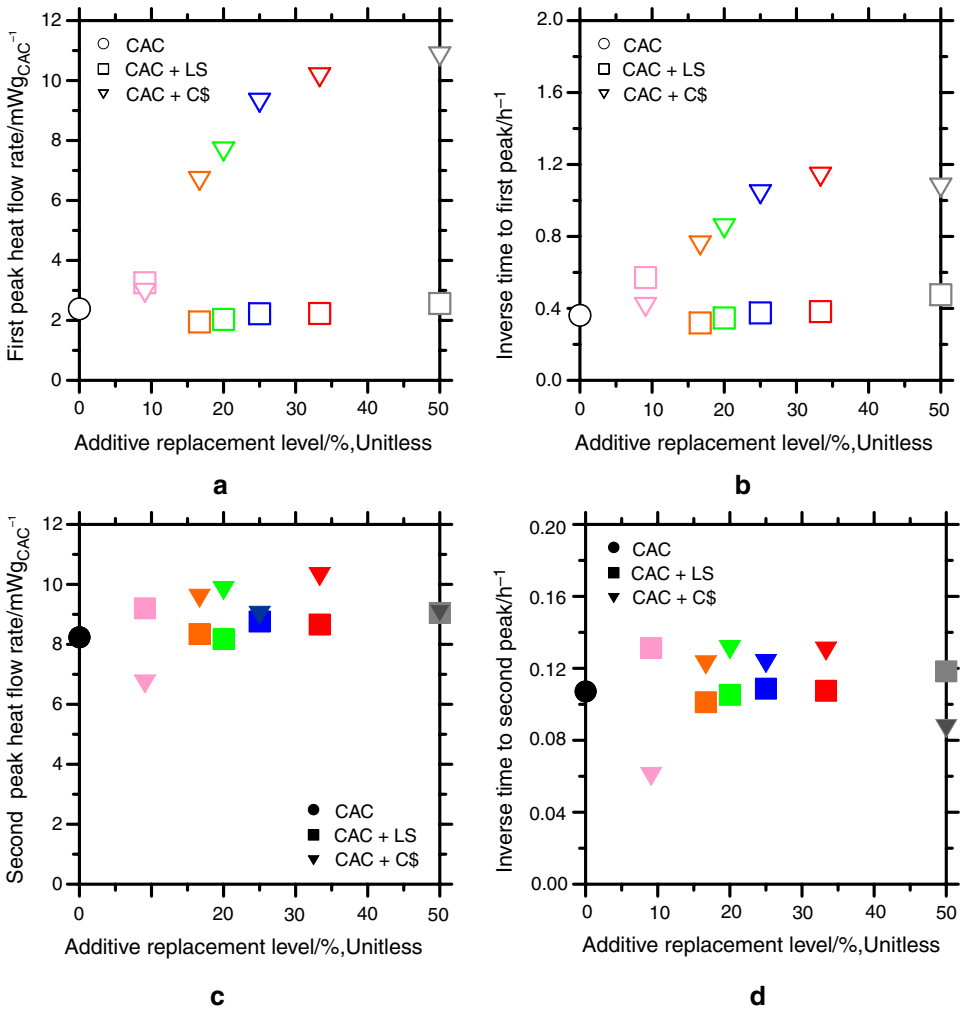

Fig. 4 Peak heat flow rate and inverse time to the peak extracted from the calorimetry curves for CAC, [CAC + C$], and [CAC + LS] pastes. **a**, **b** are the peak heat flow rate and inverse time to peak for the first hydration peak, whereas **c** and **d** are the same parameters but for the second hydration peak

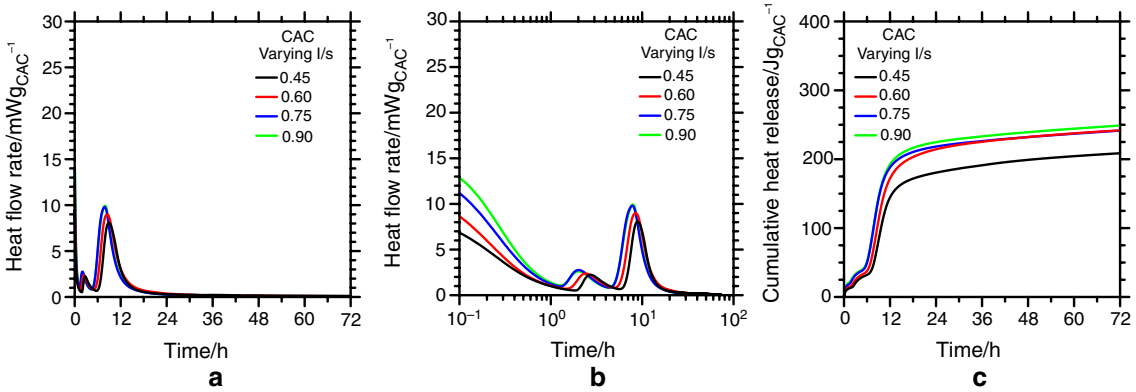

Fig. 5 Calorimetry profiles of CAC pastes hydrated with increasing water-to-cement (w/c) ratio: **a** heat flow rate up to 72 h and linear x-axis, **b** heat flow rate with logarithmic x-axis, **c** cumulative heat release

or heterogenous nucleation by a passivation mechanism (e.g., protective barrier layer, heterogenous nucleation of hydrates onto surface sites, or ionic complexes as seen in [C_3A + C$] systems [29–31, 41]).

In both binary systems, there was an increase in the cumulative heat release as the replacement levels increases. Although the effectiveness of the coarse limestone to accelerate CAC appears minimal in these systems, there is a

monotonic increase in the cumulative heat release (i.e., the reactivity per gram of CAC) with the 50% LS replacement level releasing 334.6 J g_{CAC}^{-1}, whereas the [CAC + C$] paste released 373.2 J g_{CAC}^{-1} after the 72-h period. While hemicarboaluminate or monocarboaluminate hydrate species can form in the presence of LS in these conditions, LS dissolution in cementitious conditions can be described as kinetically limited since the dissolution rates are on the order of 10 nm h^{-1} when submerged in a 12 pH solution [44]. Likewise, the work of Puerta-Fall et al. [9] showed via thermal analysis that the residual amount of unreacted LS in a CAC mixture with a 10% LS replacement level was ≈ 70% for 3 days and ≈ 60% for 7 days while about 50% LS remains after hydrating for 90 days.

Therefore, this increase in the cumulative heat release could not be wholly attributed to increased effectiveness in LS to heterogeneously nucleate hydrates nor LS readily participating in the hydration reaction. But as the LS content increases, a greater fraction of LS will replace CAC allowing a greater amount of water available to react with the residual anhydrous CAC powder and subsequently incorporate into the hydroxyl-AFm phases as well as some carbonate-based AFm hydrates. While increasing the *l*/*s* in OPC systems has little effect on the hydration kinetics during the early stages of hydration [46, 47], there is evidence that increasing the *l*/*s* ratio in pure CAC systems as well as [C_3A + C$\bar{S}H_2$] systems increases heat flow rate [30, 31, 48]. Figure 5 presents the calorimetry curves of pure CAC pastes with increasing water content and comparable results as seen in the literature are obtained where the calorimetry profile is slightly enhanced with increasing *l*/*s*. This manifests in a slight leftward shift in both hydration peaks, and an increase in the cumulative heat release as the *l*/*s* increases in the pure CAC paste. Therefore, increasing the LS or C$ replacement level in the binary paste consequently increases the effective water-to-cement (*w*/*c**) ratio (i.e., the amount of CAC cement decreases as replacement level increases even though the amount of water remains the same resulting in the phenomena described as the dilution effect [49, 50]). It can be surmised that the enhancements seen in the [CAC + LS] pastes and [CAC + C$] pastes calorimetry can be attributed to a combination of chemical and physical factors of the additives as well as the dilution effect.

To gain an understanding of degree of hydration of the pastes, calorimetry was conducted on pure CAC paste with a 0.45 *l*/*s* for a duration of 10 days. After the 10 days, the cumulative heat release was 242.481 J g^{-1}_{CAC} which was used to quantify the degree of hydration (α, the fraction of CAC reacted). For the pure CAC pastes with varying *l*/*s*, the values of α increase from 0.861, 0.998, 0.996, and 1.000 for 0.45, 0.60, 0.75, and 0.90, respectively.

This process was used previously for mixtures of C_3S and pozzolanic additives for a 24-h hydration period [23, 24]. However, the longer time periods as well as the addition of LS and C$ prompt a much greater cumulative heat release than the pure CAC paste observed previously. Therefore, instead of using the cumulative heat release of the pure CAC paste, the cumulative heats released of the binary pastes were extrapolated to 10 days to determine α. The calculated values of α for the C$ and LS binary pastes are presented in Table 2.

Compared to the pure CAC paste, the value of α changes depending on the additive in the binary system. The addition of coarse limestone slightly lowers α compared to the neat CAC paste. Conversely, after three days the [CAC + C$] pastes exhibit almost near completion indicating acceleration in the hydration kinetics compared to the neat CAC.

Coupling these calculated values of α and the GEMS simulations, the phase composition present in microstructure at three days can be estimate as a function of α as presented in Fig. 6. For the sake of simplicity and for direct comparison to the later experiments, the pure CAC paste and the 17%, the 25%, and the 50% replacement levels for both the [CAC + LS] and [CAC + C$] systems are shown. The formation of hydrotalcite forms due to the small amount of magnesia present in the CAC, whereas the other constituent oxides (e.g., Fe_2O_3 or SiO_2) are assumed to substitute in the AFm phases or hydrogarnet phases.

As shown in Fig. 6a, the GEMS simulation does not show any conversion process; rather, the simulation has the overall reaction (i.e., Eq. 3) occurring throughout the hydration of CAC. This can be attributed to how the software calculates the steps before the reaction is completed. Each step of the hydration reaction in GEMS is based on a series of equilibrium steps before reaching an $\alpha = 1.0$. While C_3AH_6 does not form outright from CA at 20 °C, the C_2AH_8 and CAH_{10} will eventually convert into C_3AH_6 obtaining equilibrium. For the binary pastes, the difference in α between the [CAC + LS] and [CAC + C$] pastes becomes apparent due to the difference in dissolution rates of LS and C$. As shown in Fig. 6b–d, LS is calculated to remain in the microstructure throughout the duration of the CAC hydration, whereas for

Table 2 Degree of hydration of the binary pastes for the different [CAC + LS] and [CAC + C$] pastes after hydrating for 72 h

Replacement level of additive/%	Degree of reaction (α)	
	[CAC + LS] Pastes	[CAC + C$] Pastes
9	0.825	0.990
17	0.799	0.955
20	0.797	0.926
25	0.813	0.983
33	0.823	0.956
50	0.832	0.952

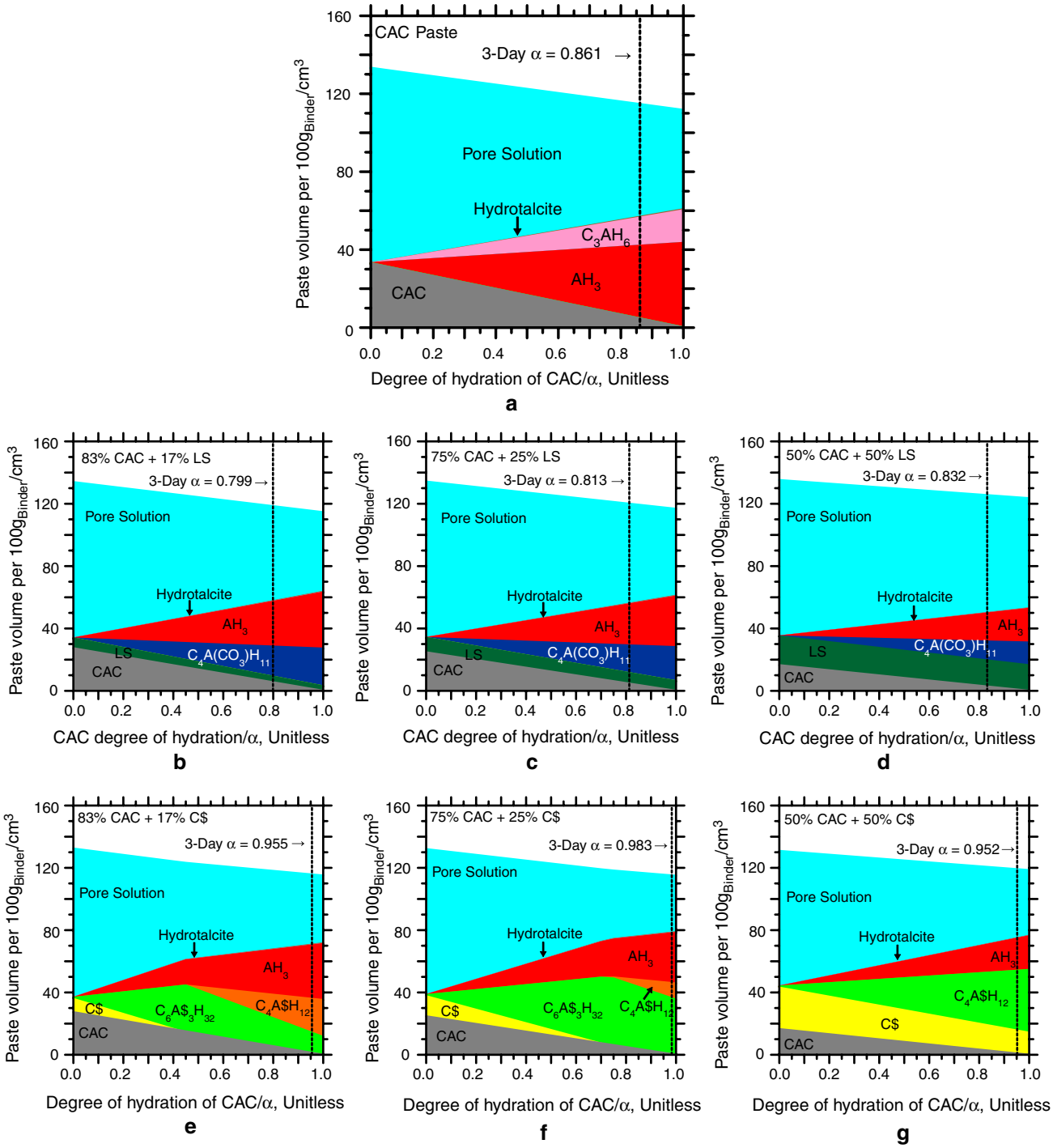

Fig. 6 A series of GEMS simulations for the **a** pure CAC paste, **b**–**d** 17%, 25%, and 50% LS replacement levels as well as **e**–**g** 17%, 25%, and 50% C$ replacement with excess water (1:1 total solid-to-liquid mass ratio)

the [CAC + C$] pastes, the C$ is calculated to completely dissolve except at the 50% replacement level.

Examining the [CAC + LS] pastes, the GEMS simulations predict a reduction of AH_3 due to the reduction in CAC. The simulation does not predict any of the hydroxyl-AFm or CAH_{10} coexisting with the monocarboaluminate phase which is contradicting experimental observations herein in Fig. 7 or from the literature [9, 10]. This can be attributed to the limited solubility of the LS and how this insolubility kinetically limits the amount of monocarboaluminate present in the microstructure [9]. Although these calcium aluminate hydrates are permitted to form in the simulation, the addition

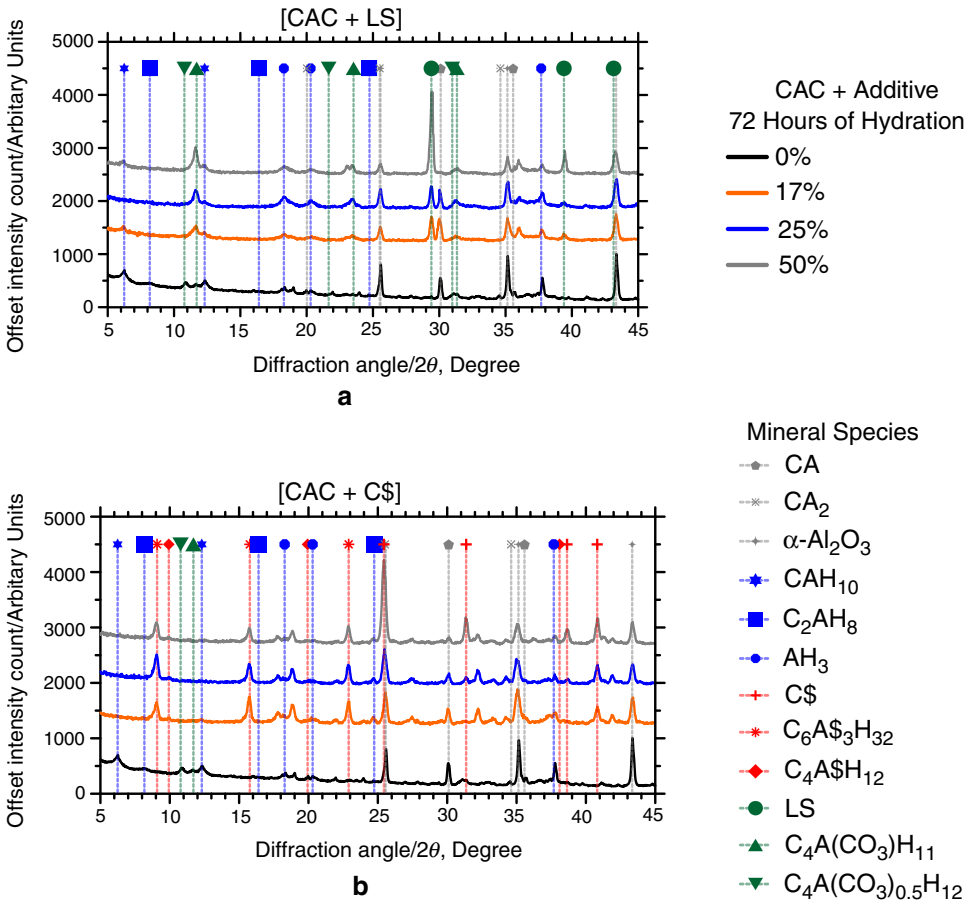

Fig. 7 XRD patterns of **a** [CAC + LS] and **b** [CAC + C$] paste after 72 h of hydration. The diffraction patterns are ordered so that the bottom is the pure CAC paste while the higher diffractograms are of higher replacement level

of LS prevents the formation of these phases because in part the formation of monocarboaluminate hydrate would reduce Gibb's free energy of the system more so than the metastable phases and therefore prevent the latter from forming.

The microstructure of the [CAC + C$] paste is expected to be comparable to expansive calcium sulfoaluminate cements in which ettringite and aluminum hydroxide are considered the main hydration products [51]. These results are replicated in the thermodynamic simulations showing these hydrates being the most prominent in the GEMS simulations as well as monosulfoaluminate phase being present in the 17% and 25% C$ replacement level. The presence of monosulfoaluminate for the 17% and 25% replacement levels collaborates the idea that third peak seen in the inset of Fig. 3 corresponds to monosulfoaluminate formation. Similarly, within that inset of Fig. 3b, the magnitude of the third peak is greater for the 17% than the 25% which indicates increased growth of monosulfoaluminate in the microstructure.

The XRD patterns show that the phase composition of the paste is not as consolidated as the GEMS simulations calculated previously in Fig. 6 for both singular and binary pastes. The only calcium aluminate hydrate phase detected in the pure CAC pastes was CAH_{10} in addition to residual CA and CA_2 that remained unreacted. Since the limestone did not facilitate the complete removal of the CAH_{10}, the remaining CAH_{10} could undergo the "conversion" process as described in the introduction like the pure CAC paste. On the topic of the pure CAC paste, slight carbonation of the sample leads to the formation of hemicarboaluminate ($C_4A(CO_3)_{0.5}H_{12}$) and monosulfoaluminate perhaps transforming any C_2AH_8 that would have formed due to the greater thermodynamic stability of the carbonate phases. Moreover, there are some weak diffraction peaks corresponding to AH_3 (particularly at lower diffraction angles 18.28° and 20.30°) in both systems, but this could be due to the amorphous nature of the phase. As the limestone content increases (as shown with the increase in intensity and sharpening of the diffraction peak at 29.408°), the hemicarboaluminate diffraction peak disappears while the monocarboaluminate peak intensity increases albeit the number of counts does not increase by large degree.

The hydration products present in the [CAC + C$] pastes are like the GEMS simulations with ettringite ($C_6A\$_3H_{32}$) and monosulfoaluminate ($C_4A\$H_{12}$) and AH_3 being the product phases between three different C$ replacement levels. The ettringite peak appears to be the sharpest for the 25% C$ paste rather than the 50% C$ replacement level.

For the monosulfoaluminate, the 11 molar H_2O species was detected in all three replacement levels albeit with a low intensity count. The 14 molar H_2O monosulfoaluminate hydrate (PDF# 00-042-0062) [52–54] was not detected in the diffractograms of the [CAC + C$] paste. However, all three replacement levels for [CAC + C$] pastes contain XRD peaks corresponding to C$. This indicates that the complete dissolution of C$ does not occur, and therefore, a different mechanism instead of the depletion of C$ is responsible for the C$ not affecting the second hydration peak. Moreover, none of the diffraction peaks associated with the calcium aluminate hydrates are detected in the [CAC + C$] pastes which can be attributed to the presence of SO_4^{2-} ions facilitating the formation of ettringite and/or monosulfoaluminate rather than the metastable CAH_{10} or C_2AH_8 phases. This is similar to previous observations by Son et al. where they replaced CAC with 8% C$ (for a CAC mortar) and observed limited formation of CAH_{10} [13]. Therefore, the 17% C$ [CAC + C$] system appears to be sufficient in preventing the "conversion" process from occurring. For additional examination, the XRD results are be cross-examined with the DTGA results in Fig. 8.

Starting with the DTGA scan corresponding to the pure CAC paste, the paste exhibits mass losses near 120 °C and later near ≈ 280 °C. These are characteristic temperatures of the dehydroxylation of CAH_{10} and AH_3 according to Scrivener et al. [55] which collaborates the XRD results presented previously in Fig. 7. Conversely, the [CAC + LS] pastes prompt a peak before 200 °C as well as a second peak between 200 and 320 °C. This corresponds with the dehydroxylation of monocarboaluminate which occurs via two steps process. First, the chemically bound water within the interlayer becomes liberated at temperatures before 200 °C. Afterwards, the remaining chemically bound water is released between 200 and 300 °C. Since the mass loss rate of the first interlayer water from the monocarboaluminate species appears similar, the remaining mass loss rate at the second stage would be attributed to the monocarboaluminate and the AH_3 present. As expected, the decomposition rate of LS increased between 600 and 800 °C as the LS replacement level increases, showing that a significant amount of LS remains after three days hydrating. The 17% LS replacement exhibits a slightly increase in mass loss rate at ≈ 280 °C compared to the other LS replacement levels.

Conversely, the [CAC + C$] pastes exhibit a sharp mass loss rate at ≈ 100 °C with similar mass loss rates at 200–300 °C as the neat CAC paste. The first mass loss peak is the dehydroxylation of the water molecules from the ettringite structure, and since ettringite can contain 26 mol of chemically bounded H_2O per molecule, this contributes to a high mass loss rate [55]. After the dehydroxylation of ettringite, the remaining water bounded to the aluminum hydroxide is removed between 200 and 300 °C which reflects similar DTGA signal as the pure CAC pastes. The 25% C$ paste exhibited the highest mass loss rate during the first stage corresponding the XRD results in Fig. 7b. Conversely for the second decomposition stage, it was the 17% replacement level which exhibited the lowest dehydroxylation rate at ≈ 100 °C but a slightly higher DTGA signal associated with AH_3 between 200 and 300 °C. However, all three of the [CAC + C$] pastes exhibited a lower DTGA signal than the pure CAC paste. While the XRD results showed that monosulfoaluminate is present in the microstructure of the [CAC + C$] pastes, the amount appears to be overshadowed by the mass loss rates corresponding to the other hydrates. Conversely, while the higher C$ replacement levels prompt acceleration for the first hydration peak (see Fig. 4), it does not lead to an increase in the amount of ettringite at 72 h. Rather, there is residual C$ remaining in the microstructure after 72 h, as seen in the XRD results. The acceleration of the first hydration peak could originate from energetically

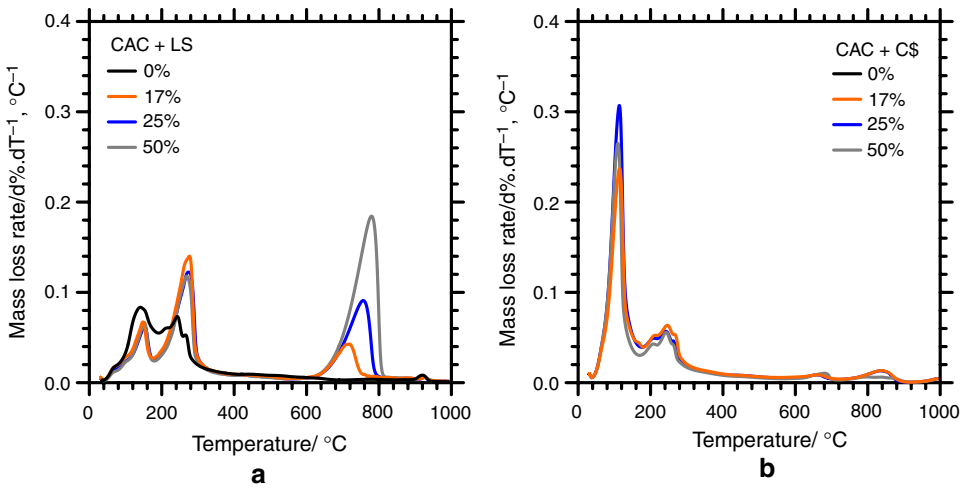

Fig. 8 DTGA scans of **a** [CAC + LS] pastes and **b** [CAC + C$] pastes from 0 to 1000 °C for 0%, 17%, 25%, and 50% replacement level, respectively

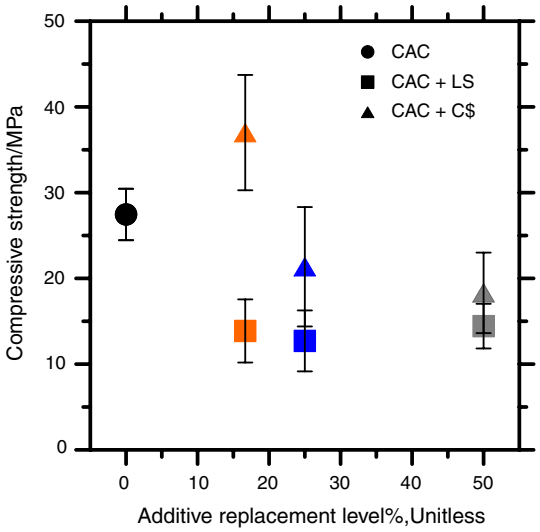

Fig. 9 Strength of the 6 mm side length cubic samples with the standard deviation shown as error bars

favorable nucleation sites on the C$ surface, but later for the second hydration peak the surface effects are minimized.

The compression strength results for the CAC pastes are presented in Fig. 9. The [CAC + LS] pastes exhibit a decrease in strength compared to the pure CAC paste with an average strength ranging from 12 to 15 MPa compared to the 27.45 MPa ± 3.001 MPa of the pure CAC paste. In contrast, the [CAC + C$] pastes exhibit higher strengths than the [CAC + LS] counterparts. Although the 25% C$ and 50% C$ replacement levels prompt a greater amount of ettringite as depicted in DTGA (Fig. 8), it does not appear that increasing the amount of ettringite correlates with strength gain. In fact, the paste containing 17% C$ replacement level exhibits the greatest compressive strength with 37.00 MPa ± 6.725 MPa (while having less ettringite than 25% C$ and 50% C$ replacement levels) and is the only paste to exhibit strength increase compared to the pure CAC paste. How this strength increase translates to the fired sample is unclear. Ettringite undergoes a complex decomposition process initially forming bassanite and sulfoaluminate phases, and subsequently, the sulfoaluminate phase will decompose into katoite (C_3AH_6) [56, 57]. The excess water released during this process can be detrimental to bulk properties. As previously mentioned, CA-25 C is utilized for high-temperature applications and contains α-Al_2O_3 as a mineral additive. α-Al_2O_3 has compressive strengths × 10 higher than conventional concrete as catalogued in Appendix C of Ashby [58]. Therefore, the reduction in the amount of α-Al_2O_3 by replacing the CAC with LS or C$ (both of which exhibit much lower Mohs hardness levels than α-Al_2O_3; 3 and 3.5 compared to 9, respectively) will reduce the strength of the bulk material.

Conclusions

Replacing high-α-Al_2O_3 calcium aluminate cement (CAC) with limestone or calcium sulfate greatly changed the hydration kinetics of the CAC paste. The limestone exhibited limited benefits to the hydration kinetics of the CAC system in part to coarseness of the powder. For the two hydration peaks, there was no positive nor negative correlation in the peak heat flow rate or the time to that peak as the limestone replacement level increased. The coarse particle size distribution prevented any enhanced heterogenous nucleation and growth (i.e., filler effect) due to the limited reactive surface area, and the intrinsic insolubility kinetically limits the formation of monocarboaluminate phases allowing CAH_{10} to form. Conversely, the cumulative heat release increased as the limestone content increased; however, this was not due to any enhanced reactivity provided by the limestone rather the increase in the amount of water available to reactive with CAC via the dilution effect. The GEMS simulations overestimated the effect that LS had on the phase composition predicting monocarboaluminate would destabilize the formation of metastable CAH_{10} or C_2AH_8, whereas the phase composition was shown via XRD and DTGA to contain a mixture of metastable calcium aluminate hydrate hydrates and the monocarboaluminate hydrate.

In comparison, the increase in the C$ replacement levels accelerated the early hydration CAC kinetics (i.e., the first hydration peak). There are several compounding effects provided by C$ that could accelerate the hydration kinetics of CAC such as the heat generated by dissolution of C$ or the heterogenous nucleation of ettringite on the C$ surface. But the results herein provide evidence that C$ acts as an effective material for the heterogenous nucleation of ettringite and appears to be the dominating mechanism for the first hydration peak. If the acceleration was due to the dissolution of C$, then it would be expected that more ettringite would form due to increase in sulfate ions present in the microstructure. This is not the case however, because the 25% C$ replacement level formed more ettringite than the [CAC + C$] paste with 50% C$ replacement level as shown in XRD and DTGA. Additionally, the 17%, 25%, and 50% replacement level exhibited evidence that C$ remained in the microstructure after the 72-h hydration period in contrast to the thermodynamic simulations. The simulations were accurate predicting the lack of any hydroxyl-AFm phase (notably CAH_{10}) in the [CAC + C$] mixtures which would prevent the "conversion" process as seen in normal CAC mixtures; however, the simulations predicted similar outcome for the [CAC + LS] systems which did not materialize in the observations. The replacement level of C$ does not strongly influence the peak heat

flow rate or the time to the second hydration peak although C$ is present in the microstructure. While the exact mechanism for C$ not affecting the second hydration peak is not clear and additional investigations can elucidate this, the presence of C$ after the 72-h hydration period indicates that any acceleratory benefits provided by C$ earlier in the hydration reaction is reduced and/or removed after the first peak. Both sets of binary pastes exhibited higher cumulative heat released, but this did not result in benefits in the strength of the bulk material. Only the paste containing 17% C$ exhibited a positive effect on the compressive strength, whereas the remaining binary pastes exhibited compressive strengths less than the pure CAC pastes. It is unclear how this strength increase would translate to the dried or fired sample since the ettringite would decompose into monosulfoaluminate and later C_3AH_6 during these processes. While ettringite exhibits cementing properties, as seen in calcium sulfoaluminate systems, the increase in ettringite did not translate in an increase in compressive strength of the sample. It is expected that the amount of hydrates nor residual unreacted LS or C$ cannot compensate for the decrease in strength by reducing the α-Al_2O_3 content present in the CAC.

Acknowledgements Funding for this study was provided by the National Science Foundation (CMMI: 1661609 and CMMI: 1932690). Experiments were conducted at the Materials Research Center and the Center for Infrastructure Engineering Studies at Missouri S&T.

Declarations

Conflict of interest The authors declare that they have no conflict of interest.

References

1. Scrivener KL, Cabiron J-L, Letourneux R. High-performance concretes from calcium aluminate cements. Cem Concr Res. 1999;29(8):1215–23.
2. Parreira RM, Andrade TL, Luz AP, Pandolfelli VC, Oliveira IR. Calcium aluminate cement-based compositions for biomaterial applications. Ceram Int. 2016;42(10):11732–8.
3. Scrivener K. Calcium aluminate cements. In: Advanced concrete technology. 1st ed. Burlington: Butterworth-Heinemann; 2003. p. 2/1–2/30. https://books.google.com/books?id=CL4G4fPDHGkC
4. Matschei T, Lothenbach B, Glasser FP. The AFm phase in Portland cement. Cem Concr Res. 2007;37(2):118–30.
5. Baquerizo LG, Matschei T, Scrivener KL, Saeidpour M, Wadsö L. Hydration states of AFm cement phases. Cem Concr Res. 2015;73:143–57.
6. Luz AP, Pandolfelli VC. $CaCO_3$ addition effect on the hydration and mechanical strength evolution of calcium aluminate cement for endodontic applications. Ceram Int. 2012;38(2):1417–25.
7. Rashid S, Barnes P, Turrillas X. The rapid conversion of calcium aluminate cement hydrates, as revealed by synchrotron energy-dispersive diffraction. Adv Cem Res. 1992;4(14):61–7.
8. Klaus SR, Neubauer J, Goetz-Neunhoeffer F. Hydration kinetics of CA2 and CA—investigations performed on a synthetic calcium aluminate cement. Cem Concr Res. 2013;43:62–9.
9. Puerta-Falla G, Balonis M, Le Saout G, Kumar A, Rivera M, Falzone G, et al. The influence of slightly and highly soluble carbonate salts on phase relations in hydrated calcium aluminate cements. J Mater Sci. 2016;51(12):6062–74.
10. Puerta-Falla G, Kumar A, Gomez-Zamorano L, Bauchy M, Neithalath N, Sant G. The influence of filler type and surface area on the hydration rates of calcium aluminate cement. Constr Build Mater. 2015;96:657–65.
11. Bizzozero J, Scrivener KL. Limestone reaction in calcium aluminate cement–calcium sulfate systems. Cem Concr Res. 2015;76:159–69.
12. Falzone G, Balonis M, Sant G. X-AFm stabilization as a mechanism of bypassing conversion phenomena in calcium aluminate cements. Cem Concr Res. 2015;72:54–68.
13. Son HM, Park S, Kim HY, Seo JH, Lee HK. Effect of $CaSO_4$ on hydration and phase conversion of calcium aluminate cement. Constr Build Mater. 2019;224:40–7.
14. Meyn M, Beneke K, Lagaly G. Anion-exchange reactions of layered double hydroxides. Inorg Chem. 1990;29(26):5201–7.
15. Newman SP, Jones W. Synthesis, characterization and applications of layered double hydroxides containing organic guests. New J Chem. 1998;22(2):105–15.
16. Rousselot I, Taviot-Guého C, Leroux F, Léone P, Palvadeau P, Besse J-P. Insights on the structural chemistry of hydrocalumite and hydrotalcite-like materials: investigation of the series $Ca_2M^{3+}(OH)_6Cl{\cdot}2H_2O$ (M^{3+}: Al^{3+}, Ga^{3+}, Fe^{3+}, and Sc^{3+}) by X-ray powder diffraction. J Solid State Chem. 2002;167(1):137–44.
17. Chrysochoou M, Dermatas D. Evaluation of ettringite and hydrocalumite formation for heavy metal immobilization: literature review and experimental study. J Hazard Mater. 2006;136(1 spec. iss.):20–33.
18. Glasser FP, Kindness A, Stronach SA. Stability and solubility relationships in AFm phases: Part I. Chloride, sulfate and hydroxide. Cem Concr Res. 1999;29(6):861–6.
19. Baquerizo LG, Matschei T, Scrivener KL, Saeidpour M, Thorell A, Wadsö L. Methods to determine hydration states of minerals and cement hydrates. Cem Concr Res. 2014;65:85–95.
20. Damidot D, Stronach S, Kindness A, Atkins M, Glasser FP. Thermodynamic investigation of the $CaO–Al_2O_3–CaCO_3–H_2O$ closed system at 25°C and the influence of Na_2O. Cem Concr Res. 1994;24(3):10.
21. Gutteridge WA, Dalziel JA. Filler cement: The effect of the secondary component on the hydration of Portland cement: Part I. A fine non-hydraulic filler. Cem Concr Res. 1990;20(5):853–61.
22. Oey T, Kumar A, Bullard JW, Neithalath N, Sant G. The filler effect: the influence of filler content and surface area on cementitious reaction rates. J Am Ceram Soc. 2013;96(6):1978–90.
23. Lapeyre J, Kumar A. Influence of pozzolanic additives on hydration mechanisms of tricalcium silicate. J Am Ceram Soc. 2018;101(8):3557–74.
24. Lapeyre J, Ma H, Kumar A. Effect of particle size distribution of metakaolin on hydration kinetics of tricalcium silicate. J Am Ceram Soc. 2019;102(10):5976–88.
25. Cook R, Ma H, Kumar A. Influence of size-classified and slightly soluble mineral additives on hydration of tricalcium silicate. J Am Ceram Soc. 2020;103(4):2764–79.
26. Klaus SR, Neubauer J, Goetz-Neunhoeffer F. Influence of the specific surface area of alumina fillers on CAC hydration kinetics. Adv Cem Res. 2016;28(1):62–70.
27. Berodier E, Scrivener K. Understanding the filler effect on the nucleation and growth of C–S–H. J Am Ceram Soc. 2014;97(12):3764–73.

28. Kumar A, Oey T, Falzone G, Huang J, Bauchy M, Balonis M, et al. The filler effect: the influence of filler content and type on the hydration rate of tricalcium silicate. J Am Ceram Soc. 2017;100(7):3316–28.
29. Minard H, Garrault S, Regnaud L, Nonat A. Mechanisms and parameters controlling the tricalcium aluminate reactivity in the presence of gypsum. Cem Concr Res. 2007;37(10):1418–26.
30. Quennoz A, Scrivener KL. Hydration of C3A–gypsum systems. Cem Concr Res. 2012;42(7):1032–41.
31. Joseph S, Skibsted J, Cizer Ö. A quantitative study of the C3A hydration. Cem Concr Res. 2019;115:145–59.
32. Garboczi EJ, Bullard JW. Shape analysis of a reference cement. Cem Concr Res. 2004;34(10):1933–7.
33. Bullard JW, Garboczi EJ. A model investigation of the influence of particle shape on portland cement hydration. Cem Concr Res. 2006;36(6):1007–15.
34. Zhang J, Scherer GW. Comparison of methods for arresting hydration of cement. Cem Concr Res. 2011;41(10):1024–36.
35. Zhang Z, Scherer GW. Evaluation of drying methods by nitrogen adsorption. Cem Concr Res. 2019;120:13–26.
36. Scrivener K, Snellings R, Lothenbach B, editors. A practical guide to microstructural analysis of cementitious materials. CRC Press; 2018.
37. Lothenbach B, Kulik DA, Matschei T, Balonis M, Baquerizo L, Dilnesa B, et al. Cemdata18: a chemical thermodynamic database for hydrated Portland cements and alkali-activated materials. Cem Concr Res. 2019;115:472–506.
38. Kulik DA, Wagner T, Dmytrieva SV, Kosakowski G, Hingerl FF, Chudnenko KV, et al. GEM-Selektor geochemical modeling package: revised algorithm and GEMS3K numerical kernel for coupled simulation codes. Comput Geosci. 2012. https://doi.org/10.1007/s10596-012-9310-6.
39. Wagner T, Kulik DA, Hingerl FF, Dmytrieva SV. GEM-Selektor geochemical modeling package: TSolMod library and data interface for multicomponent phase models. Can Mineral. 2012;50(5):1173–95.
40. Lapeyre J, Ma H, Okoronkwo M, Sant G, Kumar A. Influence of water activity on hydration of tricalcium aluminate-calcium sulfate systems. J Am Ceram Soc. 2020. https://doi.org/10.1111/jace.17046.
41. Myers RJ, Geng G, Li J, Rodríguez ED, Ha J, Kidkhunthod P, et al. Role of adsorption phenomena in cubic tricalcium aluminate dissolution. Langmuir. 2017;33(1):45–55.
42. Geng G, Myers RJ, Yu Y-S, Shapiro DA, Winarski R, Levitz PE, et al. Synchrotron X-ray nanotomographic and spectromicroscopic study of the tricalcium aluminate hydration in the presence of gypsum. Cem Concr Res. 2018;111:130–7.
43. Myers RJ, Geng G, Rodriguez ED, da Rosa P, Kirchheim AP, Monteiro PJM. Solution chemistry of cubic and orthorhombic tricalcium aluminate hydration. Cem Concr Res. 2017;100:176–85.
44. Pignatelli I, Kumar A, Field KG, Wang B, Yu Y, Le Pape Y, et al. Direct experimental evidence for differing reactivity alterations of minerals following irradiation: the case of calcite and quartz. Sci Rep. 2016;6:20155.
45. Evju C, Hansen S. The kinetics of ettringite formation and dilatation in a blended cement with β-hemihydrate and anhydrite as calcium sulfate. Cem Concr Res. 2005;35(12):2310–21.
46. Ley-Hernandez AM, Lapeyre J, Cook R, Kumar A, Feys D. Elucidating the effect of water-to-cement ratio on the hydration mechanisms of cement. ACS Omega. 2018;3(5):5092–105.
47. Scrivener K, Ouzia A, Juilland P, Kunhi Mohamed A. Advances in understanding cement hydration mechanisms. Cem Concr Res. 2019;124:105823.
48. Chotard T, Gimet-Breart N, Smith A, Fargeot D, Bonnet JP, Gault C. Application of ultrasonic testing to describe the hydration of calcium aluminate cement at the early age. Cem Concr Res. 2001;31(3):405–12.
49. Bonavetti V, Donza H, Menéndez G, Cabrera O, Irassar EF. Limestone filler cement in low w/c concrete: a rational use of energy. Cem Concr Res. 2003;33(6):865–71.
50. Bentz DP. Modeling the influence of limestone filler on cement hydration using CEMHYD3D. Cem Concr Compos. 2006;28(2):124–9.
51. Habert G. 10—Assessing the environmental impact of conventional and 'green' cement production. In: Pacheco-Torgal F, Cabeza LF, Labrincha J, de Magalhães A, editors. Eco-efficient construction and building materials. Woodhead Publishing; 2014. p. 199–238.
52. Poellmann H, Kuzel H. 00-042-0062. International Centre for Diffraction Data; 2019.
53. Kuzel H-J, Pöllmann H. Hydration of C3A in the presence of $Ca(OH)_2$, $CaSO_4{\cdot}2H_2O$ and $CaCO_3$. Cem Concr Res. 1991;21(5):885–95.
54. Pollmann H. Solid solution in the system 3CaO. Al2O3. CaSO4. aq-3CaO. Al2O3. Ca (OH) 2. aq-H2O at 25 degree C, 45 degree C, 60 degree C, 80 degree C. Naegele U Obermiller, Science Publishers, Johannesstrasse 3A, D 70176 Stuttgart, Germany: E Schweizerbartsche Verlags; 1989. p. 27–40.
55. Scrivener K, Snellings R, Lothenbach B, editors. Thermogravimetric analysis. In: A practical guide to microstructural analysis of cementitious materials. CRC Press; 2018. https://www.taylorfrancis.com/books/9781498738675
56. Hall C, Barnes P, Billimore AD, Jupe AC, Turrillas X. Thermal decomposition of ettringite $Ca_6[Al(OH)_6]2(SO_4)3{\cdot}26H_2O$. J Chem Soc Faraday Trans. 1996;92(12):2125–9.
57. Meller N, Kyritsis K, Hall C. The hydrothermal decomposition of calcium monosulfoaluminate 14-hydrate to katoite hydrogarnet and β-anhydrite: An in-situ synchrotron X-ray diffraction study. J Solid State Chem. 2009;182(10):2743–7.
58. Ashby MF. Materials selection in mechanical design. 3rd ed. Amsterdam: Butterworth-Heinemann; 2005.